ACS APPLIED NANO MATERIALS

www.acsanm.org Article

Ca/Fe-Based Nanozymes Relieve Severe Acute Pancreatitis by Ferroptosis Regulation and Reactive Oxygen Species Scavenging

Yuhang Li,[▽] Rui Cai,[▽] Kang Chen, Yujing Zhang, Xu Chen, Bo Sun, Yu Jiang, Chaochao Tan, Chuang Peng, Yinghui Song,* Ling Wu,* and Sulai Liu*

Cite This: *ACS Appl. Nano Mater.* 2023, 6, 12968−12979 Read Online

ACCESS | Metrics & More | Article Recommendations | Supporting Information

ABSTRACT: Severe acute pancreatitis (SAP) is a serious inflammatory disease that is often associated with high mortality rate. It tends to trigger a cascade of systemic inflammation that causes damage to multiple organs, such as the lungs and kidneys. Currently, there is no effective treatment plan to reverse the progress of SAP. The occurrence and development of SAP are associated with oxidative stress (OS) and ferroptosis. In this study, the Ca/Fe-based nanozymes are used as multi-enzyme simulants, which can effectively remove the reactive oxygen species and regulate ferroptosis to prevent and treat SAP. Notably, we make two trials for prevention and treatment of SAP. Under the condition of good biocompatibility, the Ca/Fe-based nanozymes effectively reduce the levels of serum pancreatitis-related biomarkers and inflammatory factors which involved in local and systemic inflammatory response. Moreover, the Ca/Fe nanozymes significantly increase the level of ferroptosis regulator of glutathione peroxidase 4 (GPx4) and ferritin heavy chain 1 (FTH1) in pancreas. These results demonstrate that the Ca/Fe-based nanozymes not only alleviate SAP but also mitigate subsequent multi-organ damage, thus providing an effective strategy of Ca/Fe nanozymes for treating SAP-related disorders in clinical research.

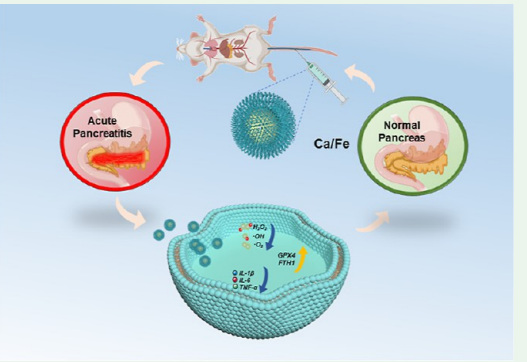

KEYWORDS: *severe acute pancreatitis, antioxidant stress, Ca/Fe-based nanozymes, treatment, prevention*

1. INTRODUCTION

Acute pancreatitis (AP) is a frequent acute abdomen in gastroenterology, which has the characteristics of acute onset, severe illness, and rapid change.[1−3] Around 20−30% of AP patients will develop serious diseases to severe acute pancreatitis (SAP) and have a higher mortality rate with a short period of time.[4,5] In SAP, the activation of pancreatic enzymes is often accompanied by pancreatic digestion, swelling, bleeding, and necrosis.[6] Unfortunately, SAP could eventually cause damage to multiple organ functions in the body, especially influencing the lungs, kidneys, and liver.[7,8] At present, the treatment of SAP is mainly through targeted management of generalized complications.[6,9] Although treatment options for SAP have been extensively studied, there has been no significant improvement in clinical outcomes for SAP-related patients. Given that there are no clinically approved definitive medicines to treat SAP, the development of a novel and efficient intervention strategy for SAP treatment is an urgent demand.[10]

Oxidative stress (OS) plays a major role in SAP, causing several macrophages to penetrate the inflammatory area.[11,12] Both NADPH oxidase and mitochondrial dysfunction are the major causes of OS in SAP, and hydrogen peroxide (H_2O_2), as the second messenger of NADPH oxidase, is the major source of reactive oxygen species (ROS) in inflammation.[13,14] Subsequently, OS can further spread the local and systemic inflammation resulting from the activation of neutrophils' inflammatory response to acinar cell injury.[15] As a form of regulation of programmed cell death, ferroptosis is involved in the damage process of acinar cells in SAP, which can disrupt the balance between ROS production induced by iron accumulation and the antioxidant system within lipid peroxidation.[16,17] As a lipid repair enzyme, GPX4 is a key factor of ferroptosis, and the dysfunction or abnormal level of FTH1 will cause an increase in intracellular iron amount, allowing us to promote the occurrence of ferroptosis.[16,18] However, research of SAP treatment is still at a preliminary stage of exploration, and the development of novel nanozyme-based drugs for inhibition of ferroptosis to protect organs in SAP remains to be challenging.

Nanozymes are functional nanomaterials with enzyme-like activity. These nanomaterials have a catalytic mechanism similar to natural enzymes and can catalyze the oxidation of the

Received: April 16, 2023
Accepted: June 26, 2023
Published: July 13, 2023

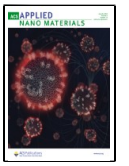

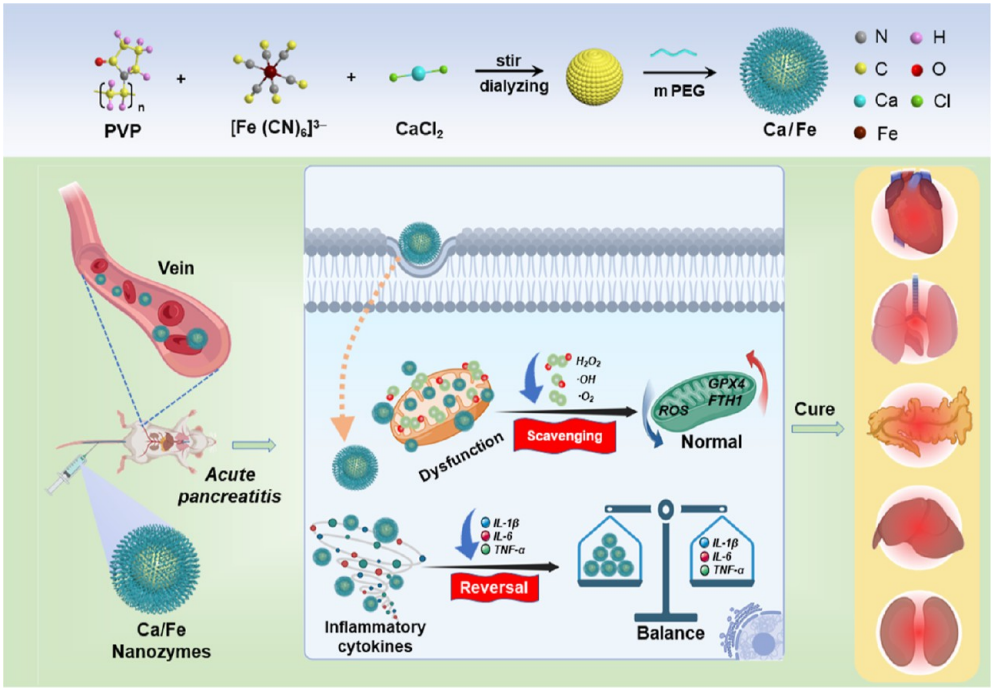

Figure 1. Schematic diagram of the mechanism of Ca/Fe-based nanozymes treating SAP.

natural enzyme substrate.[19−21] Many important achievements have been made in the research of nanoenzymes, which have shown considerable application value in the biomedical field in recent years.[22−24] Nanozymes with endogenous enzyme-mimicking catalytic activity have been considered innovative drugs for the treatment of ROS-related diseases.[25,26] Among them, Prussian blue (PB) nanoparticles present excellent biocompatibility, photoacoustic/photothermal conversion, and multi-enzyme mimetic activity, which are considered to be effective scavengers of ROS.[27,28] PB nanozymes with superoxide dismutase (SOD)- and peroxidase (POD)-simulated activity can convert excess harmful oxygen radicals into harmless products.[29] The biological applications of PB nanozymes are studied in many diseases, including osteoporosis,[30] radiation-induced hematopoietic injury,[31] experimental lung adenocarcinoma, and anthracycline-induced liver injury.[32] However, the mechanisms of nanozymes in the treatment of ROS-related SAP remain unclear; it is of significance to develop novel nanozymes and deeply understand the therapeutic mechanism for the achievement of therapeutic applications.

Herein, we report a Prussian blue analogue nanocatalyst of Ca/Fe nanozymes via a facile environmental strategy (Figure 1). The as-prepared Ca/Fe nanozymes present a uniform well-dispersed spherical morphology with an ultrasmall average size of ∼7.5 nm, which was beneficial to cross through the cell membranes. Importantly, the Ca/Fe-based nanozymes possessed not only excellent antioxidant capability but also anti-inflammatory activity that can induce the regulation of the expression of inflammatory factors without obvious toxicity. We also studied the antioxidant multi-enzyme nanocatalytic performance of Ca/Fe nanozymes in vitro and in vivo. The synthesized Ca/Fe nanozymes can show good therapeutic potential for SAP, thus revealing its further biomedical application potential in the treatment of diseases related to inflammation and OS.

2. MATERIALS AND METHODS

2.1. Reagents and Instrumentation. All reagents were acquired from formal commercial suppliers. Potassium hexacyanoferrate(III) ($K_3[Fe(CN)_6]$), 3,3′,5,5′- tetramethylbenzidine (TMB), and pyrogallol were bought from Shanghai Aladdin Bio-Chem Technology Co., Ltd. Mal-PEG_{2000}-COOH was bought from Xi'an ruixi Biological Technology Co. Ltd. Calcium chloride ($CaCl_2$), iron(II) sulfate heptahydrate ($FeSO_4·7H_2O$), sodium nitrite ($NaNO_2$), tris-(hydroxymethyl) aminomethane (Tris), glutathione (GSH), hydrogen peroxide (H_2O_2), and hydrochloric acid (HCl) were bought from Sinopharm Chemical Reagent Co., Ltd. Polyvinylpyrrolidone (PVP) was purchased from Chengdu Alcorta Chemical Reagent Co., Ltd. 2,2-Diphenyl-1-picrylhydrazyl (DPPH), glutathione reductase (GR), and tetracyclohexanamine (NADPH) were bought from Macklin Biochemical Technology Co., Ltd. Caerulein was purchased from APEXBIO. All operations on mice in this study were approved by the Institutional Animal Committee of Hunan Provincial People's Hospital (The First Affiliated Hospital of Hunan Normal University).

We used a UV−vis spectrophotometer (1900i, Shimadzu, Japan) to record the UV−vis absorption spectra. We used a Nicolet iS20 spectrometer (Thermo Fisher Scientific, USA) to measure Fourier transform infrared (FTIR) spectroscopy. We used a JEM-F200 (JEOL, Japan) to obtain the transmission electron microscopy (TEM) images and EDS spectra. The zeta potential data was recoded on a nanoparticle analyzer (90 Plus Zeta, Brookhaven Instruments, USA). The elemental valence states of nanozymes were measured by X-ray photoelectron spectroscopy (XPS) (Thermo Scientific K-Alpha, USA).

2.2. Preparation of Ca/Fe Nanozymes. The solution of 20 mL of 10 mM calcium chloride ($CaCl_2$) was added to 20 mL of 10 mM $K_3[Fe(CN)_6]$ to obtain a homogeneous solution. The solution was then placed in a round-bottom flask. 500 mg of polyvinyl pyrrolidone (PVP) was dropped to produce a yellow solution under stirring for 25 min at room temperature. The resulting solution was transferred to a dialysis bag (M = 12,000) for the treatment of 2 h. The deionized water for dialysis was replaced after 30 min every time, and the solution was frozen overnight at −20 °C to collect products. After thawing the product, Mal-$mPEG_{2000}$-COOH (10 mg) was added under stirring in the dark for 4 h. The Ca/Fe nanozyme was collected after keeping it overnight at 60 °C in an oven.

https://doi.org/10.1021/acsanm.3c01697
ACS Appl. Nano Mater. 2023, 6, 12968−12979

2.3. Assay of SOD-like Activity. The determination of SOD-like activity was evaluated by inhibition of the pyrogallol autoxidation method. Typically, 0.5 mL of 50 mM Tris-HCl (pH = 8.6) and 10 μL of pyrogallol were added into the test tube for 3 min in a water bath at 25 °C, which produces the autoxidation rate of pyrogallol to $O_2^{\bullet-}$. The inhibition of the pyrogallol autoxidation was examined by the addition of Ca/Fe nanozymes at different concentrations (400, 600, 800, and 1000 μg/mL) into the test tube for 3 min in a water bath at 25 °C. The absorption inhibition rate and the autoxidation rate of pyrogallol were determined at 325 nm every 30 s for 5 min at 25 °C. We combined the UV−vis absorption spectrum and eq 1 to calculate the SOD sample of Ca/Fe-based nanozymes

$$\text{Inhibition rate} = \Delta A_0 - \Delta A_{SOD}/\Delta A_0 \times 100\% \quad (1)$$

where ΔA_0 is the difference in absorbance per 30 s in the control group (buffer + pyrogallol) and ΔA_{SOD} is the difference in absorbance per 30 s in the experimental group (buffer + Ca/Fe nanozyme + pyrogallol).

2.4. POD-like Activity. The POD-like ability of Ca/Fe nanozymes was determined by adding the TMB solution and a nanoenzyme substrate into H_2O_2 solution. Briefly, 800 μL of PBS solution, 100 μL of 50 mM H_2O_2 solution, 100 μL of Ca/Fe nanozymes, and 40 mM TMB were mixed and transferred into a cuvette, and then the absorption of the assay solution was recorded at 652 nm.

2.5. GPx-like Ability. The glutathione peroxidase (GPx)-like ability of Ca/Fe nanozymes was analyzed through oxidizing glutathione (GSH) to glutathione (GSSG) in the detection system of H_2O_2. The phosphate buffer (50 mM; pH = 7.4) containing GSH (2 mM), NADPH (0.4 mM), GR (100 units/mg), and H_2O_2 (0.4 mM) was added into tube of the reaction system. The reaction was initiated by the addition of Ca/Fe nanozymes at different concentrations. Finally, we recorded the absorbance of the reaction solution at 340 nm.

2.6. Scavenging of RO/NSs. The scavenging of •OH was performed by the Fenton reagent method. Briefly, 85 μL of the Ca/Fe nanozyme solution at different concentrations, 7.5 mM salicylic acid, and 7.5 mmol/L ferrous sulfate solution were added into different test tubes, and finally 85 μL of the 0.01 mM H_2O_2 solution was added to start the reaction. Deionized water was added to ensure that the system volume is 1000 μL. Reaction was carried out at a constant temperature of 37 °C for 30 min, and the absorbance was obtained at 530 nm with UV−vis spectroscopy. Finally, the clearance capacity of •OH (SA) was calculated according to formula 2

$$\text{SA}\,(\%) = [1 - (A_x - A_{x0})/A_0] \times 100\% \quad (2)$$

where A_0 represents the absorbance of the control group (ferrous sulfate + salicylic acid + H_2O_2), A_x is the absorbance after adding the test sample (ferrous sulfate + salicylic acid + Ca/Fe nanozyme + H_2O_2), and A_{x0} is the absorbance of the sample itself (ferrous sulfate + salicylic acid + Ca/Fe nanozyme).

Assessment of free radical scavenging using paramagnetic resonance spectroscopy further confirms the •OH scavenging performance of Ca/Fe nanozymes. In detail, 100 mM DMPO was added into 90 mM H_2O_2 for the capture of free hydroxyl radicals, and then the Fenton reagent was dissolved in the solution to produce •OH. The scavenging ability of •OH was evaluated by electron spin resonance (ESR) amplitude intensity with or without Ca/Fe nanozymes. For the production of $ONOO^-$, 10 mL of 50 mM $NaNO_2$ solution and 10 mL of 25 mM H_2O_2 were mixed and stirred for 3 min. A yellow solution was obtained by adding a mixture solution containing HCl (5 mL, 1 M) and NaOH (5 mL, 1.5 M) within 1 s under stirring. The whole reaction system was maintained in an ice-water bath. The $ONOO^-$ scavenging capacity of Ca/Fe nanozymes was examined by the absorbance at 302 nm on UV−vis spectroscopy. For the scavenging performance of DPPH, different concentrations of Ca/Fe nanozyme solutions were added to DPPH solution (the solvent was absolute ethanol) and left in the dark for 30 min at 25 °C. Then, the absorbance values of the mixed solution were obtained at 517 nm.

2.7. Cell Cultures. Dulbecco's modified Eagle's medium (DMEM) (Gibco, China) containing 10% FBS (Gibco, China) and 1% penicillin G sodium/streptomycin sulfate was used to culture RAW264.7 cells. Ham's F-12K containing 20% FBS and 1% P/S was used to culture AR42J cells (pancreatic exocrine cells). All cell lines were placed in T-25 flasks, and cells were cultured in an incubator under 5% CO_2 at 37 °C.

2.8. Cellular Toxicity Evaluation. For Ca/Fe nanozymes, AR42J cells were preinoculated into a 96-well cell culture cluster containing fresh Ham's F-12K (190 μL) and Ca/Fe nanozymes (10 μL; 25, 50, 100, 200, 400, 800, and 1600 mg/mL). These cells were incubated for 24 h, and then the cell viability of the total culture was detected by the CCK-8 method.

2.9. Blood Compatibility Evaluation. Blood samples (2 mL) were collected from healthy people and centrifuged of 5 min at 2000 rpm. After the dispose of the upper serum, the red blood cells were washed with PBS three times for collection of red blood cell suspension (1 mL). Then. 0.1 mL of 10^9/mL red blood cells was cultured in H_2O, NaCl, DMEM, RPMI-1640, PBS, and Ca/Fe nanozyme solutions. After co-culturing for 4 h, hemolysis of the red blood cells in each group was carried out.

2.10. Ca/Fe Nanozymes Protect Cells from Oxidative Damages. RAW264.7 cells preinoculated into a 96-well cell culture cluster were incubated with 200 μL of fresh DMEM for 24 h, and then the fresh medium containing different concentrations of Ca/Fe nanozymes (25, 50, 100, 200, and 400 mg/mL) was used to treat the cells under different conditions consisting of LPS (10 μg/mL) and H_2O_2 (20 μM), separately. After the co-culturing for about 24 h, the CCK-8 method was applied to detect the cell viability of the total culture.

2.11. Live/Dead Assay of Cells. Before the preparation of the dye, the 10X assay buffer was diluted to a 10X assay buffer by ddH_2O. Then, 5 μL of calcein-AM/PI solution and 15 μL of propidium iodide solution were added to the 5 mL 1X assay buffer for the preparation of fluorescent dyes. After pretreatment under different conditions, the cells were washed with PBS three times to remove the culture medium. The fluorescent dyes were co-cultured with the cells for 15 min and then washed with PBS three times. Finally, the fluorescence images were taken using a Leica DMi8.

2.12. Intracellular ROS Detection. A DCFH-DA detector was used to determine the generation of intracellular ROS. Cells under different conditions of oxidative damage were pretreated with H_2O_2 and LPS. Subsequently, the cells were treated with DCFH-DA (10 μM) for 15 min in an incubator then washed three times with DMEM (non-FBS) to get rid of excess dye. Finally, the as-treated cells were photographed by a Leica DMi8.

After the treatment, the cells were digested by pancreatin for the preparation of single-cell suspension. An FACS Canto II was used to analyze the concentration of ROS of cells.

2.13. EdU Analysis for Cell Proliferation. The cells were cultivated in six-well plates, and the cells in different subgroups were dealt with H_2O_2 (20 μM), Ca/Fe nanozymes (200 μg/mL) with H_2O_2, LPS (10 μg/mL), Ca/Fe nanozymes (200 μg/mL) with LPS, and a negative control (PBS) for 24 h. The pretreated cells were incubated with EdU (10 μM) for 2 h under different conditions in an incubator, washed with PBS three times, co-cultivated with AlexaFluor-488 in the dark, and counterstained by DAPI. A Leica DMi8 was used to visualize the EdU-labeled DNA.

2.14. Measurements of Cytokines and Blood Indicators. For the measurements of cytokines, the ELISA experiments were conducted by using commercial kits. The RAW cells were pretreated with H_2O_2 and LPS for 24 h, and the cell supernatant was collected for further study.

Blood samples (1 mL) were collected from mice, centrifuged of 5 min at 2000 rpm, and saved the serum. For the measurements of blood indicators, the ELISA experiments were conducted by using commercial kits.

https://doi.org/10.1021/acsanm.3c01697
ACS Appl. Nano Mater. 2023, 6, 12968−12979

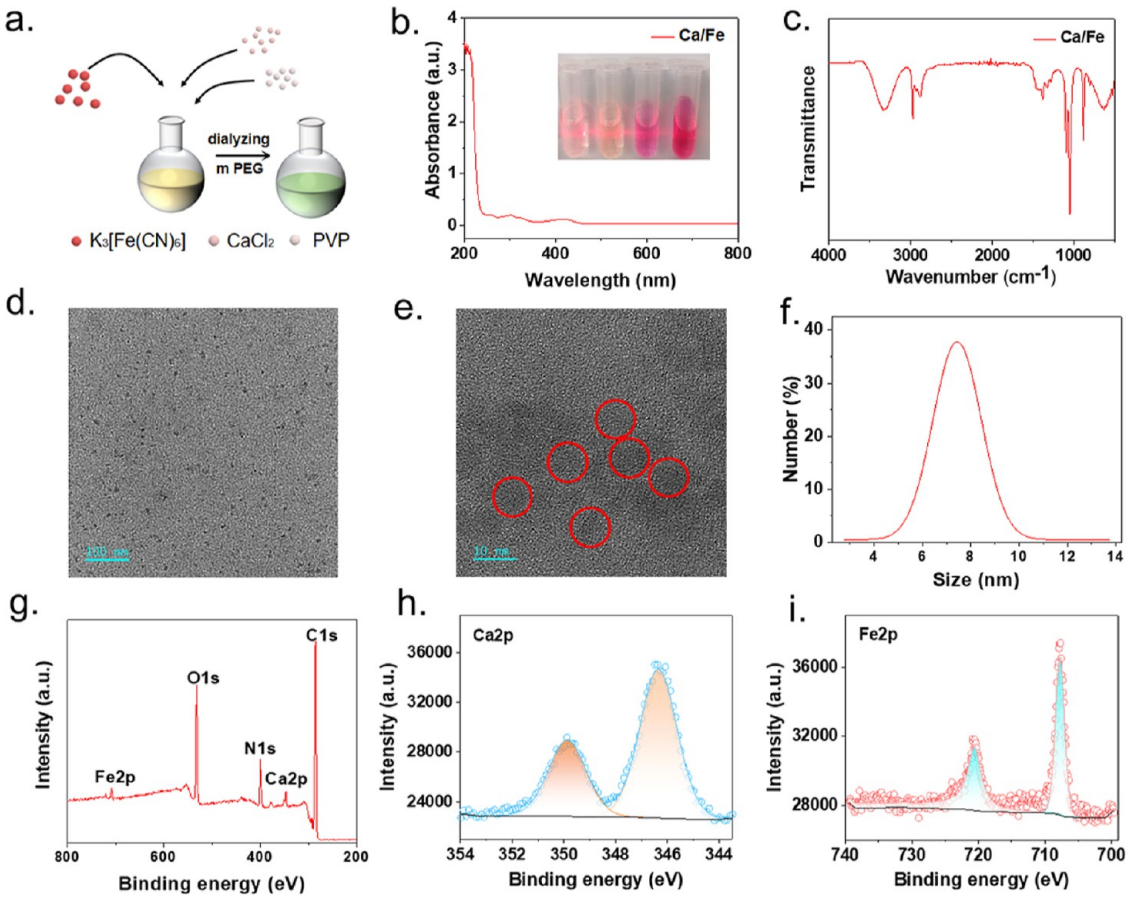

Figure 2. Synthesis and characterization of the Ca/Fe nanozymes. (a) Preparation diagram of Ca/Fe nanozymes. (b) Absorption spectrum of nanozymes dispersed in water. The inset photo is the Tyndall effect of Ca/Fe nanozymes in H_2O, PBS, RPMI-1640, and DMEM. (c) FT-IR spectrum. (d,e) TEM image of Ca/Fe nanozymes at two different scales. (f) TEM particle size statistical curve of Ca/Fe nanoparticles. (g) XPS survey spectrum of Ca/Fe nanozymes. High-resolution XPS spectrum of (h) Ca 2p and (i) Fe 2p.

2.15. Biosafety Assessment. Two groups (control and Ca/Fe group) of mice (ICR, 6-8w, female) received the treatment with NaCl or Ca/Fe nanozymes (200 μg/mL). The weights of mice were recorded for 30 days after intravenous (i.v.) injections. The serum sample was collected and stored at −80 °C. The major organs were harvested from each group. Tissues were fixed in formalin (4%) for hematoxylin and eosin (H&E) staining.

2.16. Induction of SAP Models. All the mice (ICR, 6-8w, female) were divided into three groups randomly and allowed to fast for 12 h before the experiment. The mice were treated with cerulein using intraperitoneal injections (CER, 50 μg/kg/h, seven times). After 4 h, the mice were treated with lipopolysaccharides (LPS, 10 mg/kg, 1 time) by intraperitoneal injection for the prevention and treatment of SAP mice. The control group mice were treated with sterile water (n = 6).

The SAP mice of the prevention group were intravenously administrated with Ca/Fe nanozymes at a concentration of 40 mg/kg at 19 and 23 h. The organs (pancreas, kidneys, lungs, heart, and liver) from the control and prevention group mice (n = 3) were harvested at 47 h. The SAP mice of the treatment group (n = 3) were intravenously administrated with Ca/Fe nanozymes at a concentration of 40 mg/kg in 23 and 47 h. The major organs from the control and prevention group mice were harvested at 71 h. The serum sample from the mice of the three groups was collected and stored at −80 °C.

2.17. Western Blotting. For the detection of GPX4 and FTH1 expression changes, the cell lysis buffer was used to extract the whole-cell protein of pancreas. The protein concentrations were obtained by a Micro BCA protein assay kit. The following antibodies were purchased form Cell Signaling Technology (Danvers, MA, USA): anti-GPX4 (1:1000), anti-FTH1 (1:1000), and anti-GAPDH (1:2000).

2.18. Hematoxylin and Eosin (H&E) and Immunohistochemical Staining for SAP Injury. To examine morphological and histological features, the organ tissues were fixed by paraformaldehyde (4%), paraffin-embedded, and then dehydrated and sectioned. Sections were stained with hematoxylin solution and eosin dye and then dehydrated and sealed. For inhibition of endogenous peroxidase, the sections were treated with goat serum (5%) for 30 min and incubated of 25 min with H_2O_2 (3%), followed by incubation with primary antibodies including anti-GPX4 antibody and anti-FTH1 antibody overnight at 4 °C. The next day, the horseradish peroxidase-labeled secondary antibody (1:300) was incubated for 2 h with slides at an ambient temperature. Finally, the Leica DM6 B was used for imaging analysis.

2.19. Statistical Methods. In this study, we used GRAPHPAD software to analyze the experimental data, and all data were presented by the mean ± standard deviation (SD). $p \leq 0.05$ implies the statistical significance. The standard symbols are deduced to be as $^*P \leq 0.05$, $^{**}P \leq 0.01$, $^{***}P \leq 0.001$, and ns = not significant.

3. RESULTS AND DISCUSSION

3.1. Preparation and Characterization of Ca/Fe Nanozymes. The Ca/Fe nanozyme was prepared through dissolution and reduction of the precursors of calcium chloride ($CaCl_2$) and potassium ferricyanide ($K_3[Fe(CN)_6]$) with Mal-mPEG$_{2000}$-COOH in the presence of polyvinyl pyrrolidone (PVP), as shown in Figure 2a. The as-synthesized Ca/Fe nanozyme exhibits yellow-green color in an aqueous solution

https://doi.org/10.1021/acsanm.3c01697
ACS Appl. Nano Mater. 2023, 6, 12968−12979

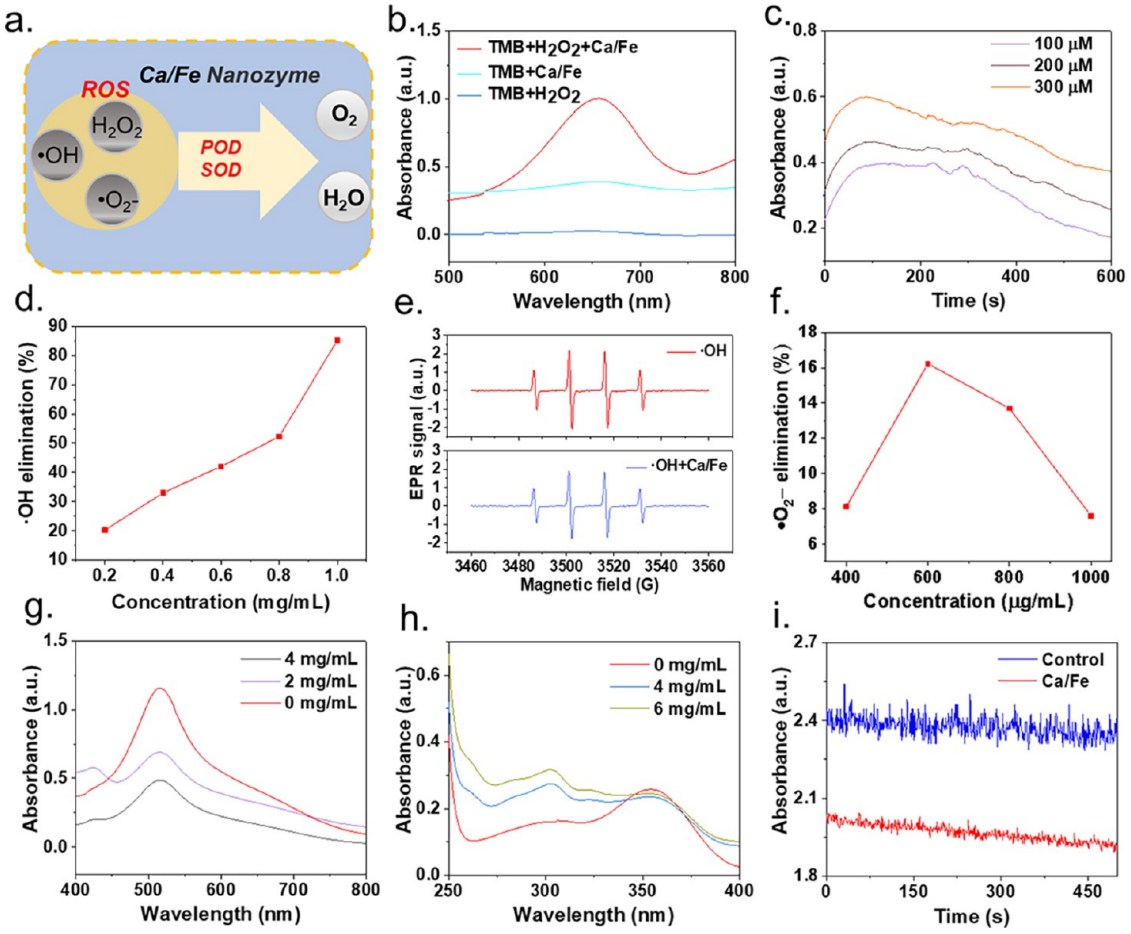

Figure 3. Antioxidant activity of Ca/Fe nanozymes. (a) The diagram represents the antioxidative activities of Ca/Fe nanozymes. (b) POD-like activity of Ca/Fe nanozymes. (c) Absorption values of TMB solution in Ca/Fe nanozymes with different amounts of H_2O_2. (d) •OH elimination using Ca/Fe nanozymes by the Fenton reagent method. (e) EPR results for •OH elimination using the Ca-Fe@PEG nanozyme. (f) SOD-like activity of Ca/Fe nanozymes. (g) RNS-scavenging capability of nanozymes for DPPH. (h) $ONOO^-$ elimination. (i) GPx-like activity of Ca/Fe nanozymes.

with strong ultraviolet absorption and excellent stability (Figure 2b). The characteristic peaks of the FT-IR pattern of the Ca/Fe nanozyme observed at 1652 and 1385 cm^{-1} were assigned to the C≡N stretching vibration and bending vibration, C═N bending vibration, and C−N out-plane bending vibration corresponding to PVP. Extensive absorption from 3200 to 3400 cm^{-1} indicates that hydroxyl groups (−OH) and amino groups (−-NH_2) exist on the sample (Figure 2c). The TEM images in Figure 2d−f confirm a unique well-dispersed spherical morphology for such as-prepared Ca/Fe nanozymes, and a uniform size of 5.62−10.39 nm was observed, which allows passage through the cell membranes. Additionally, the EDS spectrogram further confirms the composition of Fe and Ca in Ca/Fe nanozymes (Figure S1). The electronic structure and elemental composition of Ca/Fe nanozymes was further investigated using XPS technology (Figure 2g). The typical peaks assignable to the binding energies of Fe 2p, Ca 2p, O 1s, N 1s, and C 1s are identified. Figure 2h displays the high-resolution Ca 2p XPS spectra with its two divided peaks corresponding to the binding energy of 356.88 and 345.08 eV, indicating the chemical states of Ca(II) for Ca. For Fe 2p (Figure 2i), the trivalent states of Fe $2p_{3/2}$ and Fe $2p_{1/2}$ of Fe^{3+} are specified to the peaks at 731.88 and 708.68 eV, and the atomic ratio of Ca/Fe in the as-synthesized nanomaterials was deduced to be 1:1, and the anion is Cl^- ions. At the same time, the surface charges of Ca/Fe nanozymes were −6.26, −7.01, and −3.49 mV in H_2O, methanol, and ethanol, respectively (Figure S2).

3.2. Antioxidant Activity of the Ca/Fe Nanozyme. The enzyme-mimicking activities of Ca/Fe nanozymes were observed via catalytic reactions of natural enzyme substrates (Figure 3a). As one of the downstream products of superoxide dismutation, H_2O_2 is a relatively long-lived non-radical ROS.[33] The accumulation of H_2O_2 in cells has different biological effects, which is dependent on their concentrations. Low levels of H_2O_2 can induce and promote cell proliferation, while high levels of H_2O_2 damage cells. As shown in Figure 3b, the Ca/Fe nanozymes show a tiny absorption peak at 652 nm of Ox-TMB by using H_2O_2 as an electron acceptor to catalyze the oxidation of TMB substrates.[25] The weak peroxidase (POD) activity may be attributed to the inactivity in alkaline environments, which is consistent with previously reported results.[34] In addition, with the increase of H_2O_2 concentration, the catalytic capacity of Ca/Fe nanozymes also increased (Figure 3c). Hydroxyl radicals can be effectively captured by salicylic acid to generate colored substances, and its mixture has strong absorption near 530 nm. However, once a substance with scavenging effect on hydroxyl radicals is added, it resulted in a decrease in absorbance at 530 nm, which was mainly attributed to the reduction in the amount of coloring products due to the

https://doi.org/10.1021/acsanm.3c01697
ACS Appl. Nano Mater. 2023, 6, 12968−12979

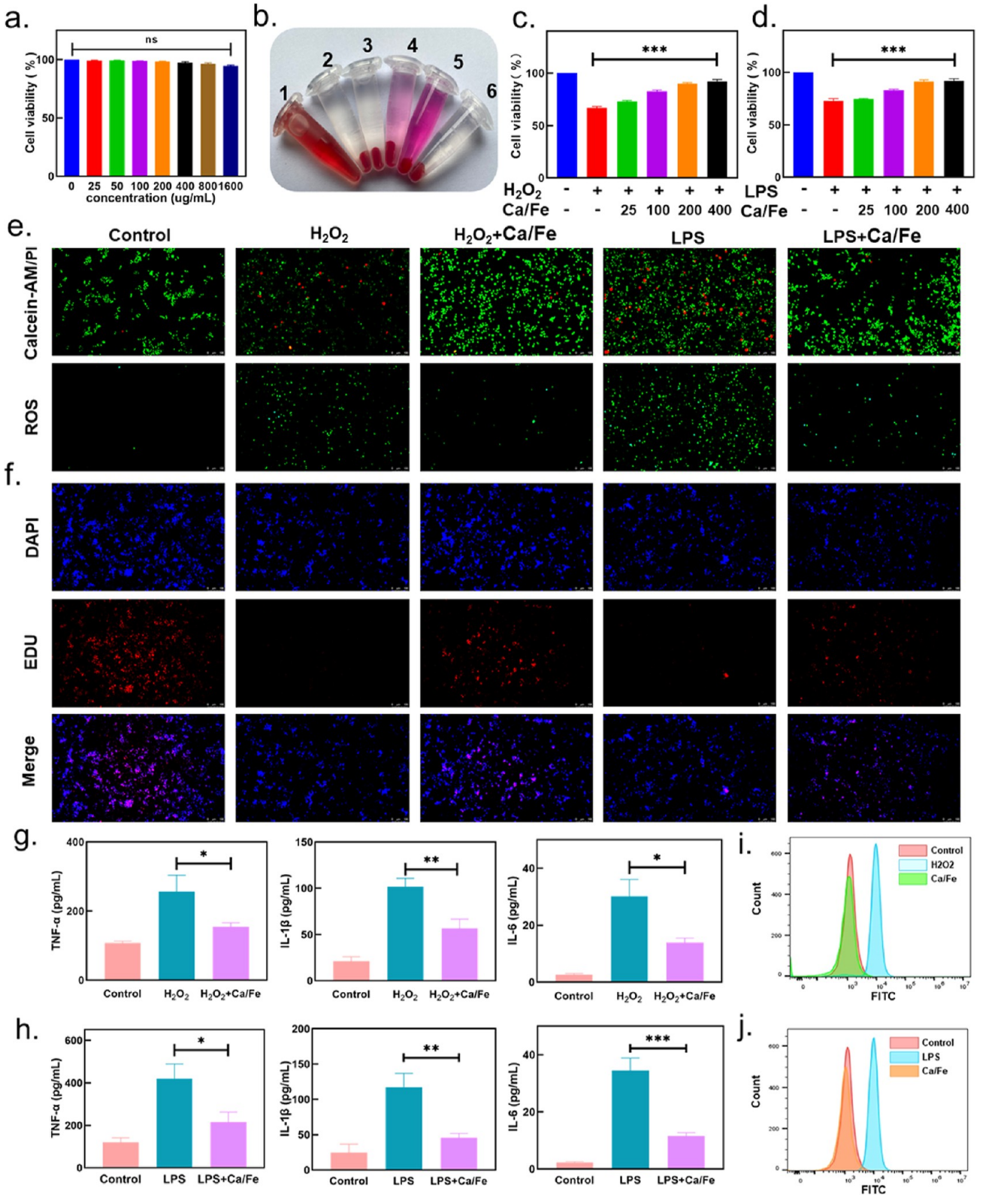

Figure 4. Safety and cytoprotective effects of Ca/Fe nanozymes. (a) Cell vitality of AR42J co-cultured at different concentrations of Ca/Fe nanozymes. (b) Photographs of hemolysis reaction of RBCs incubated with various solutions for about 4 h: (1) H_2O, (2) NaCl, (3) PBS, (4) RPMI-1640, (5) DMEM, and (6) Ca/Fe nanozymes. The Ca/Fe nanozymes protect RAW 264.7 cells from the OS caused by (c) H_2O_2 and (d) LPS. (e) Fluorescent images of RAW 264.7 cells with calcein-AM/PI stained and DCFH-DA stained after different treatments. (f) Fluorescent images of RAW 264.7 cells for proliferation with EdU stained after different treatments. Remission of inflammation and apoptosis in vitro. (g,h) Expression of inflammatory factors (TNF-α, IL-1β, and IL-6) in RAW 264.7 cells after different treatments. (i,j) Intracellular ROS levels of RAW 264.7 cells stained after different treatments were detected with DCF-DA using a flow cytometer.

https://doi.org/10.1021/acsanm.3c01697
ACS Appl. Nano Mater. 2023, 6, 12968−12979

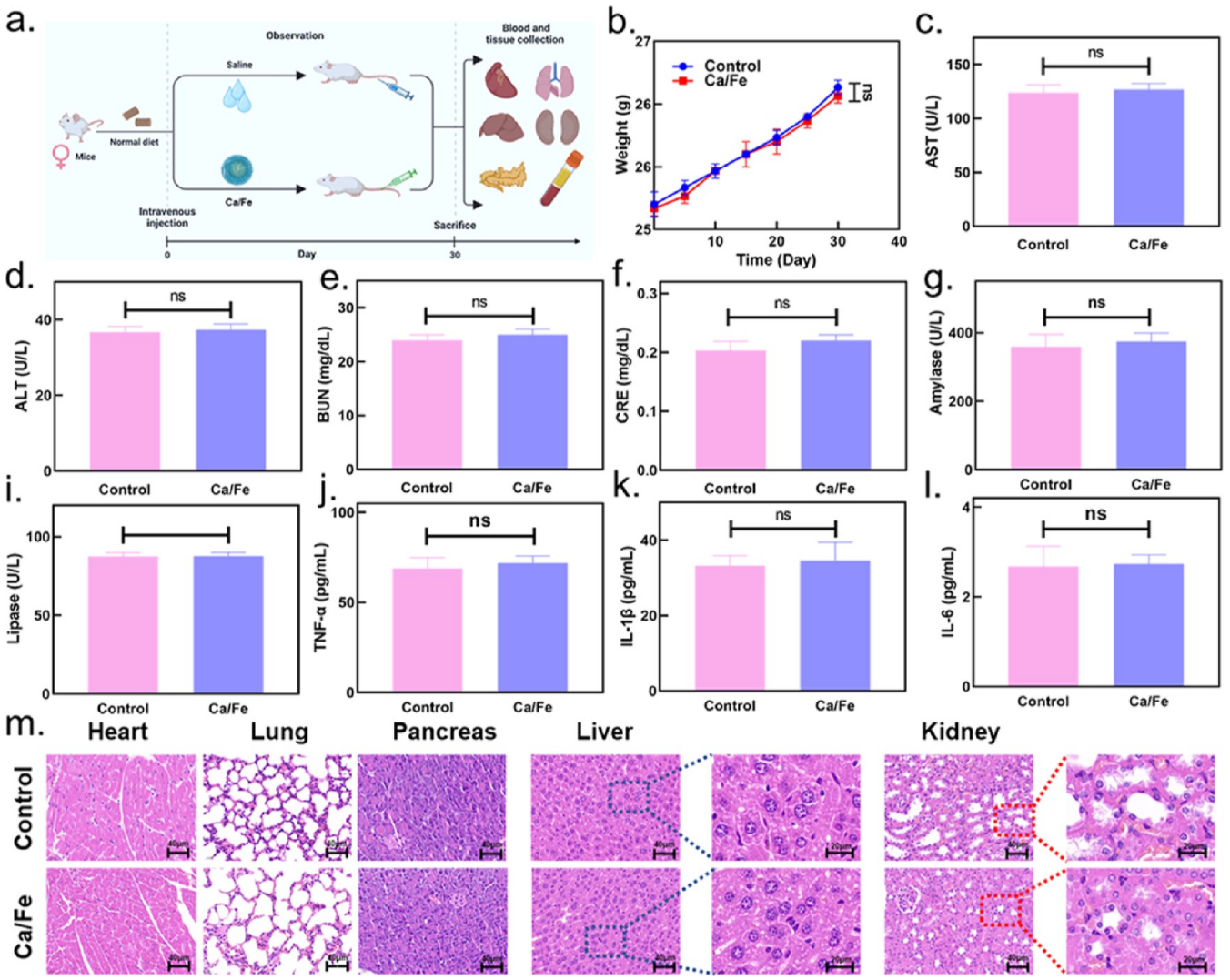

Figure 5. Histocompatibility evaluation of Ca/Fe nanozymes in vivo. (a) Operation diagram of Ca/Fe nanozymes. (b) Weight change of the mice within 30 days after the treatment of Ca/Fe nanozymes (n = 3). (c–l) Change of serum inflammatory indicators, including TNF-α, IL-1β, IL-6 amylase, and lipase in mice after the treatment of Ca/Fe nanozymes. (m) H&E staining of major organs including the pancreas, heart, liver, kidneys, and lungs in different group mice within 30 days after the treatment of Ca/Fe nanozymes.

competition with salicylic acid. There is a quantitative relationship between absorbance and radical scavenging rate. Using the Fenton reagent method according to $[1-(A_x - A_{x0})/A_0] \times 100\%$, the hydroxyl radical scavenging rate is calculated to be 85.0% at a Ca/Fe concentration of 1000 μg/mL (Figure 3d). The hydroxyl radical scavenging rate of Ca/Fe nanozymes was further monitored by ESR through amplitude reduction (Figure 3e). The superoxide anion radical is one of the shortest free radicals in human being, which can cause serious damage to cells. The superoxide dismutase in cells can scavenge the superoxide anion radical and decompose it into H_2O_2 and O_2 with low toxicity. In order to study the elimination of superoxide anion free radicals, the superoxide anion scavenging ability of nanozymes was determined by the pyrogallol autoxidation method, and the result was not significant. The superoxide anion scavenging rate was 16.24% at 600 μg/mL Ca/Fe nanozymes (Figure 3f).

As the excessive production of reactive nitrogen (RNS) is closely related to the formation of inflammation, the ability of Ca/Fe nanozymes to scavenge RNS was further studied. The 1,1-diphenyl-trihydrazide radical (DPPH•) probe in which a nitrogen radical contains many unpaired electrons was used to estimate the RNS scavenging ability of the Ca/Fe-based nanozyme (Figure 3g). In addition, to explore the ability of nanozymes to remove $ONOO^-$,[35] in order to produce $ONOO^-$, the $NaNO_2$ solution was mixed with H_2O_2, then HCl and NaOH were added, and the whole reaction system was kept in an ice-water bath. The absorbance at 302 nm for the exploration of the ability of nanozymes to remove $ONOO^-$ was measured by UV–vis spectroscopy. The experimental results show that Ca/Fe nanozymes cannot remove $ONOO^-$ (Figure 3h). Furthermore, glutathione peroxidase (GPx) has the ability to convert toxic peroxides into nontoxic hydroxyl compounds, and the GPx simulation capability of Ca/Fe nanozymes was explored (Figure 3i). Unexpectedly, no GPx simulation capability was observed in Ca/Fe nanozymes, which may be related to the reaction medium and environment of GPx activity. When the temperature is too low, the chemical activation of the material is very small. Much high temperature will cause the GPx activity escape from the composite interface before the reaction, leading to smaller response.

https://doi.org/10.1021/acsanm.3c01697
ACS Appl. Nano Mater. 2023, 6, 12968–12979

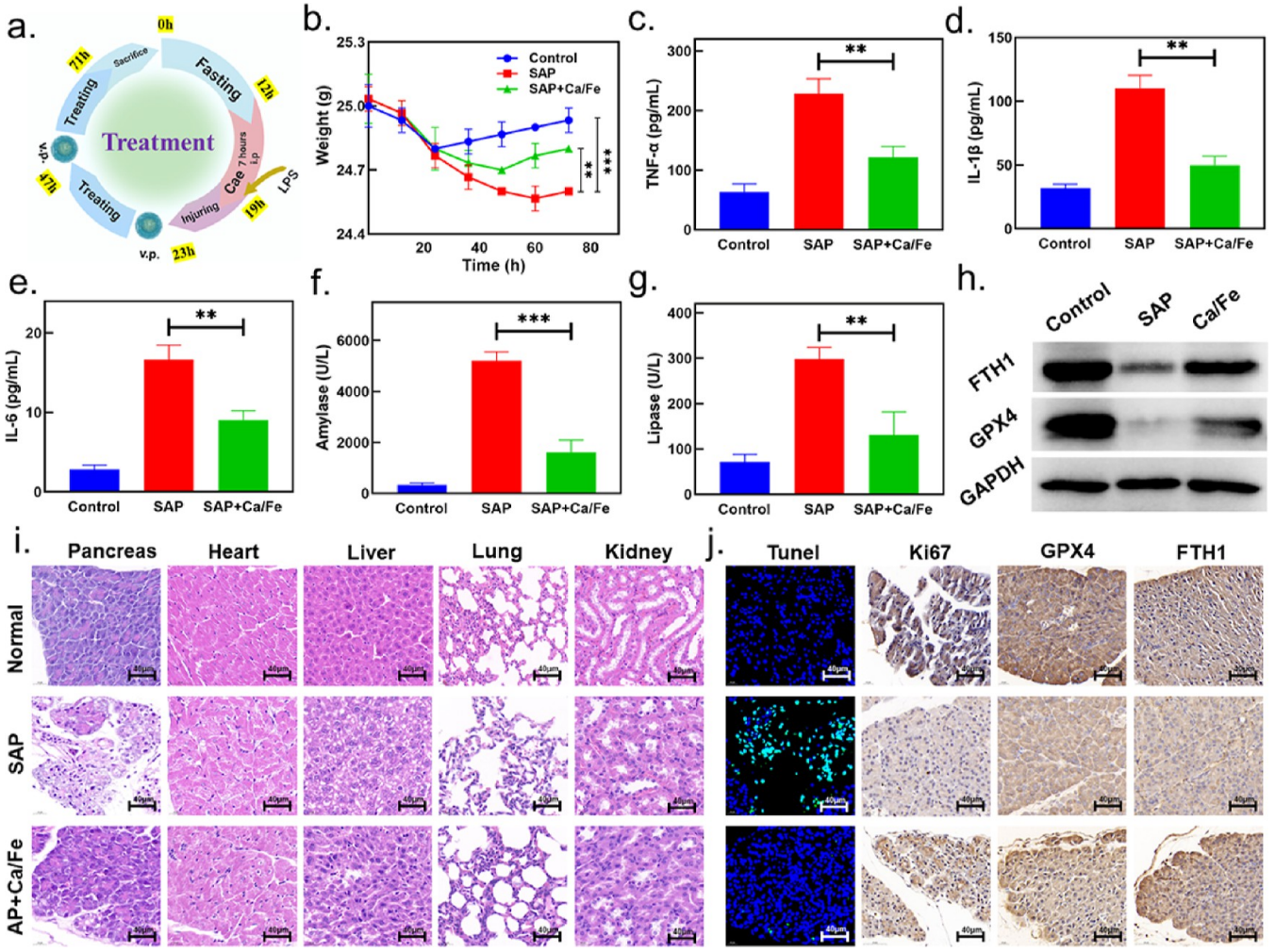

Figure 6. Treatment efficacy of Ca/Fe nanozymes for SAP mice in vivo. (a) Experimental operation diagram of treatment of Ca/Fe nanozymes in SAP mice. (b) Weight changes of different group mice recorded within 71 h (n = 3). (c–g) Change of serum inflammatory indicators, including TNF-α, IL-1β, IL-6 amylase, and lipase in mice after treatment of Ca/Fe nanozymes. (h) Western blot analysis of GPX4 and FTH1 in the pancreas of different group mice after various treatments. (i) H&E staining of major organs including the pancreas, heart, liver, kidneys, and lungs in different group mice. (j) TUNEL assay and immunohistochemical staining with GPX4, FTH1, and Ki67 in different group mice.

3.3. Safety and Cytoprotective Effects of the Ca/Fe Nanozyme. Possessing enzyme-like activities and ROS-scavenging abilities, Ca/Fe nanozymes can reduce oxidative damage in vitro and protect cells. In this study, AR42J cell lines and RAW264.7 cell lines were used to study the cytotoxicity and cytoprotective effects of Ca/Fe nanozymes. To evaluate the safety of Ca/Fe nanozymes in vitro, AR42J cells were incubated at different concentrations of Ca/Fe nanozymes for 24 h. The results of the cell counting kit-8 (CCK-8) proved that high concentrations of Ca/Fe nanozymes were not significantly toxic to cells (Figure 4a). Figure 4b shows that the red blood cells of healthy humans were incubated with different solutions (H_2O, PBS, RPMI-1640, DMED, NaCl, and Ca/Fe) for 4 h, and hemolysis was not observed in the Ca/Fe nanozyme group, indicating that it had good blood compatibility. Next, we evaluated the cellular protection of Ca/Fe nanozymes against OS produced in different ways.[36,37] Through the pretreatment of Ca/Fe nanozymes at a concentration of 200 μg/mL, the cell viability of the original cells increased from 66 to 90 and 71 to 91% (Figure 4c,d).

Moreover, the fluorescence images were captured by a fluorescence microscope and further demonstrated that through the protective effect of Ca/Fe nanozymes, cells could be protected from the toxic effects of OS produced by H_2O_2 and LPS (Figure 4e). The same result was obtained by flow cytometry (Figure 4i). Meanwhile, EdU staining is an imaging agent for cell proliferation, which can express cell value added by incorporating into newly synthesized DNA strands during cell replication. The result proved that Ca/Fe nanozymes could augment the cell-proliferating ratio after H_2O_2 and LPS treatment (Figure 4f). The cytoprotective effects of Ca/Fe nanozymes were further explored by studying the expression of cytokines in vitro. A variety of pro-inflammatory cytokines play a key role in the activation and progress of inflammation, including interleukin-1β (IL-1β), interleukin-6 (IL-6), and tumor necrosis factor-α (TNF-α). The level of cytokines was successfully reduced by treatment of Ca/Fe nanozymes (Figure 4g,h). The results showed that the Ca/Fe nanozyme mainly plays a good cytoprotective role by clearing ROS and regulating cytokines.

3.4. Histocompatibility Evaluation of Ca/Fe Nanozyme In Vivo. We verified the biocompatibility of Ca/Fe nanozymes in vivo before assessing the efficacy of Ca/Fe on SAP. After treatment with Ca/Fe nanozymes, the histocompat-

https://doi.org/10.1021/acsanm.3c01697
ACS Appl. Nano Mater. 2023, 6, 12968−12979

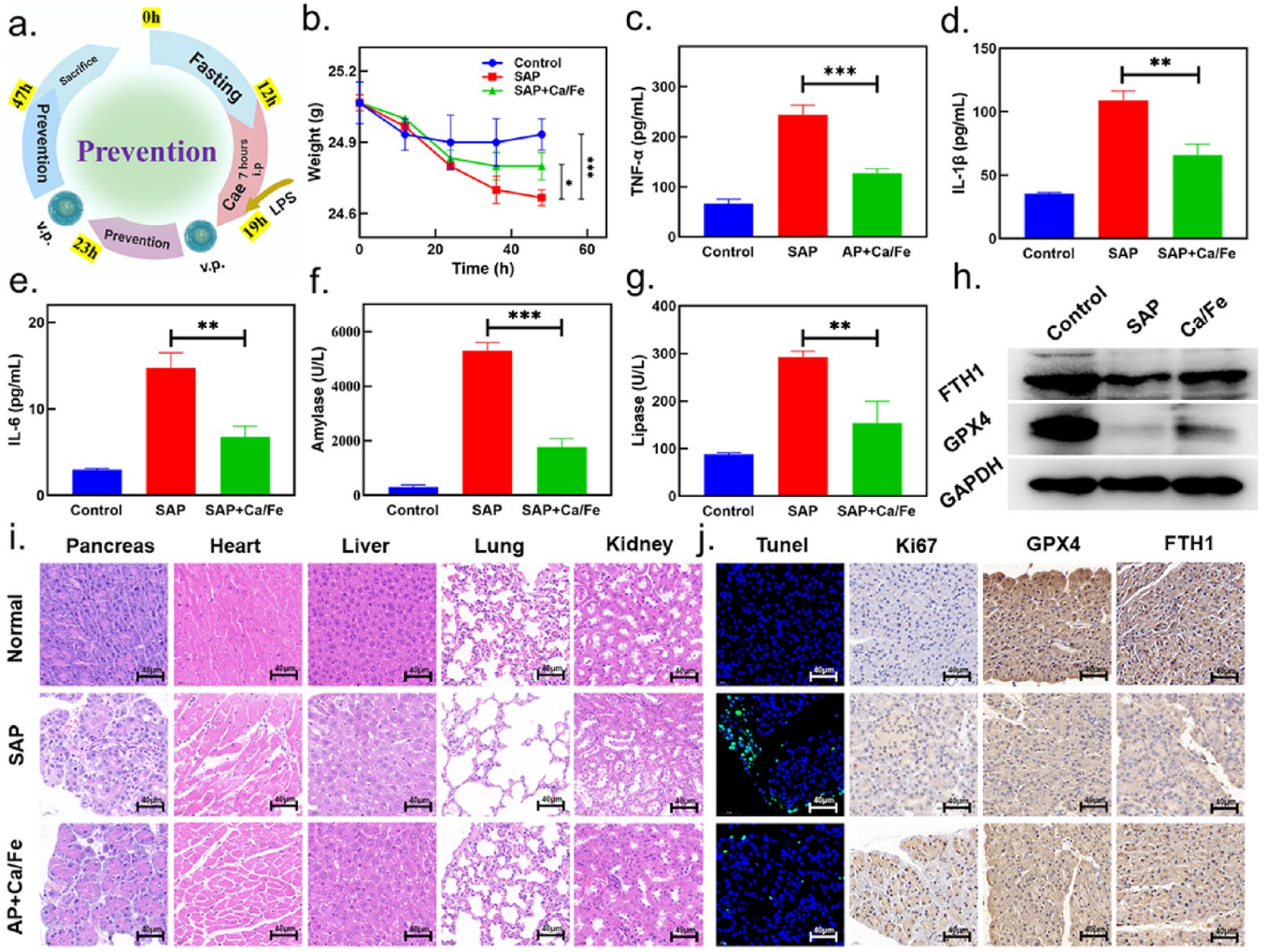

Figure 7. Prevention efficacy of Ca/Fe nanozymes for SAP mice in vivo. (a) Experimental operation diagram of prevention of Ca/Fe nanozymes in SAP mice. (b) Weight changes of different group mice recorded within 47 h (n = 3). (c–g) Change of serum inflammatory indicators, including TNF-α, IL-1β, IL-6 amylase, and lipase in mice after treatment of Ca/Fe nanozymes. (h) Western blot analysis of GPX4 and FTH1 in the pancreas of different group mice after various treatments. (i) H&E staining of major organs including the pancreas, heart, liver, kidneys, and lungs in different group mice. (j) TUNEL assay and immunohistochemical staining with GPx4, FTH1, and Ki67 in different group mice.

ibility of Ca/Fe nanozymes in vivo was evaluated by the effects on the blood biochemistry and histopathology of major organs. As shown in Figure 5a, the mice were randomly divided into two groups, and NaCl and Ca/Fe nanozymes were injected into the mice of control and Ca/Fe groups, respectively. No significant weight loss occurs after the treatment compared to the control group (Figure 5b). All hematology parameters are in the normal range after the Ca/Fe nanozyme treatment, including aspartate aminotransferase (AST), alanine aminotransferase (ALT), blood urea nitrogen (BUN), creatinine (CRE), amylase, lipase, TNF-α, IL-1β, and IL-6 (Figure 5c–l). These results indicate that Ca/Fe nanozymes cause no obvious damage to hematopoietic cells in vivo. In addition, the H&E staining images of major organs including kidneys, liver, pancreas, heart, and lungs were obtained to demonstrate the biological toxicity of Ca/Fe nanozymes. After Ca/Fe nanozyme treatment, histological evaluation showed that there were no significant morphological changes in each group, especially in the pancreas, liver, and kidneys (Figure 5m). Therefore, all the results disclose that Ca/Fe nanozymes have no obvious cytotoxicity to mice at the dose.

3.5. Treatment Efficacy of Ca/Fe Nanozymes for SAP Mice In Vivo. Besides excellent antioxidant properties and biosafety, we studied the effect of Ca/Fe nanozymes on the treatment of mice SAP. The mouse model of SAP was induced using Caerulein/LPS, and Ca/Fe nanozymes were injected according to the experimental design (Figure 6a). Three experimental groups were created, control (NaCl) group, SAP (caerulein/LPS) group, and Ca/Fe (SAP + Ca/Fe) group. To simulate the early progress of SAP, Ca/Fe nanozymes were injected during the model construction process. After Ca/Fe nanoenzyme treatment, the weight of mice showed a significant upward trend (Figure 6b). The serum sample of SAP mice was collected, and the concentration of inflammatory indicators was measured, including TNF-α, IL-1ß, IL-6, serum amylase, and lipase.[38] The results showed that the expression of various inflammatory indicators in the serum of the SAP group mice increased and that of the Ca/Fe group mice decreased significantly (Figure 6c–g). Additionally, the result of western blot proved that the occurrence of SAP would trigger the generation of ferroptosis and the negative regulation of GPX4 and FTH1. As one of the types of nonapoptotic cell death, ferroptosis is accompanied by downregulation of the

https://doi.org/10.1021/acsanm.3c01697
ACS Appl. Nano Mater. 2023, 6, 12968–12979

expression of GPX4 and FTH1, which transforms lipid hydroperoxides into lipid alcohols.[39] It was found that GPX4 and FTH1 levels returned to the control group after Ca/Fe nanozyme treatment, and the Ca/Fe group effectively attenuated ferroptosis in the pancreas of SAP mice (Figure 6h). Last, the histopathological changes were analyzed according to the H&E staining of each group of major organs (Figure 6i). Diffuse and local edema and bleeding of the pancreatic tissue in the SAP group were observed with the naked eye. After treatment with Ca/Fe nanozymes, H&E staining of the pancreatic tissue was performed, and we detected a decrease in the degree of some pathological conditions (such as interstitial pancreatic edema, neutrophil and lymphocyte infiltration, bleeding, and necrosis) than the SAP group. Meanwhile, the degree of cell damage and inflammatory cell infiltration in the liver of Ca/Fe group was reduced. The result of dT-mediated dUTP Nick-End Labeling (TUNEL) staining proved that cell apoptosis is closely linked to SAP. The obvious green-indicated cellular apoptosis was observed in the pancreas of SAP mice (Figure 6j). After Ca/Fe nanozyme treatment, the apoptosis of mouse pancreatic cells was significantly suppressed, indicating that Ca/Fe nanozymes had a good anti-apoptosis effect. Meanwhile, Ki67 staining suggested that there was more cell proliferation in the pancreas after the Ca/Fe nanozyme treatment, proving the restoration of the pancreas (Figure 6j). In addition, it is found that the levels of GPx4 and FTH1 were increased after Ca/Fe nanozyme treatment, which were similar to the control group (Figure 6j). All experimental evidence has confirmed the excellent protective properties of Ca/Fe nanozymes by regulating inflammation and inhibiting ferroptosis in SAP.

3.6. Prevention Efficacy of Ca/Fe Nanozymes for SAP Mice In Vivo. We simulated the process of prevention of SAP and constructed a novel SAP mice model. The Ca/Fe nanozyme was injected twice to observe its therapeutic effect during the construction of caerulein/LPS-induced SAP mice model (Figure 7a). The body weight of the Ca/Fe group was significantly recovered compared to the SAP group (Figure 7b). The results of all hematology parameters proved that the severity of SAP mice was reduced by the Ca/Fe nanozyme injected (Figure 7c−g). These results are a good proof that Ca/Fe nanozymes had a good preventive effect for SAP. Meanwhile, the expressions level of ferroptosis-related proteins GPX4 and FTH1 increased in the Ca/Fe group (Figure 7h). The histopathological changes of the major organs were analyzed in each group (Figure 7i). The apoptosis and proliferation of cells in pancreatic tissue were analyzed, and the expression of ferroptosis-related proteins GPX4 and FTH1 was confirmed by immunohistochemical staining results (Figure 7j). Based on the above evidence and results, the basic prevention mechanism of Ca/Fe nanozymes for SAP includes regulating inflammation and inhibiting ferroptosis.

4. CONCLUSIONS

In our study, we design a steady Ca/Fe nanozyme and simulate the effects of POD, SOD, and GPx to construct an antioxidant system that effectively removes ROS. A series of systematic studies have found that the Ca/Fe nanozyme has a comprehensive cytoprotective effect on OS in vitro, especially the ability to inhibit iron metabolism and regulate inflammation. Importantly, the excellent Ca/Fe nanozymes not only have a good ability to treat SAP and reduces damage to the pancreas and other organs but also that Ca/Fe nanozymes realize the early prevention of SAP. Further results show that inhibiting inflammation and ferroptosis are mechanisms by which caerulein-induced SAP models obtain good therapeutic effects, especially the ability to regulate cytokines, inhibit macrophage migration, and enhance the expression of GPX4. Therefore, the synthetic uniform Ca/Fe nanozyme has a strong ROS scavenging ability, advanced ferroptosis inhibition properties, and good biocompatibility. It can be used as a unique antioxidant and has an effective therapeutic effect on SAP or other diseases about OS in clinical.

■ ASSOCIATED CONTENT

Data Availability Statement

The data and materials are included in the manuscript.

Supporting Information

The Supporting Information is available free of charge at https://pubs.acs.org/doi/10.1021/acsanm.3c01697.

Additional characterization data, such as STEM with EDS mapping and surface charges (PDF)

■ AUTHOR INFORMATION

Corresponding Authors

Yinghui Song − *Central Laboratory, Hunan Provincial People's Hospital (The First Affiliated Hospital of Hunan Normal University), Changsha 410005 Hunan Province, China*; Phone: 08673183929520; Email: songyinghui@hunnu.edu.cn

Ling Wu − *Hunan Provincial Key Laboratory of Materials Protection for Electric Power and Transportation & Hunan Provincial Key Laboratory of Cytochemistry, School of Chemistry and Biological Engineering, Changsha University of Science and Technology, Changsha 410114 Hunan Province, China*; Email: wuling@csust.edu.cn

Sulai Liu − *Department of Hepatobiliary Surgery, The First Affiliated Hospital of Hunan Normal University, Changsha 410005 Hunan Province, China; Central Laboratory, Hunan Provincial People's Hospital (The First Affiliated Hospital of Hunan Normal University), Changsha 410005 Hunan Province, China; Hunan Provincial Key Laboratory of Biliary Disease Prevention and Treatment, Changsha 410005 Hunan Province, China; Clinical Medical Technology Research Center of Hunan Provincial for Biliary Disease Prevention and Treatment, Changsha 410005 Hunan Province, China*; orcid.org/0000-0002-5257-3922; Phone: 08673183929520; Email: liusulai@hunnu.edu.cn

Authors

Yuhang Li − *Department of Hepatobiliary Surgery, The First Affiliated Hospital of Hunan Normal University, Changsha 410005 Hunan Province, China; Central Laboratory, Hunan Provincial People's Hospital (The First Affiliated Hospital of Hunan Normal University), Changsha 410005 Hunan Province, China*

Rui Cai − *Hunan Provincial Key Laboratory of Materials Protection for Electric Power and Transportation & Hunan Provincial Key Laboratory of Cytochemistry, School of Chemistry and Biological Engineering, Changsha University of Science and Technology, Changsha 410114 Hunan Province, China*

Kang Chen − *Department of Hepatobiliary Surgery, The First Affiliated Hospital of Hunan Normal University, Changsha 410005 Hunan Province, China*

https://doi.org/10.1021/acsanm.3c01697
ACS Appl. Nano Mater. 2023, 6, 12968−12979

Yujing Zhang − *Central Laboratory, Hunan Provincial People's Hospital (The First Affiliated Hospital of Hunan Normal University), Changsha 410005 Hunan Province, China*

Xu Chen − *Department of Hepatobiliary Surgery, The First Affiliated Hospital of Hunan Normal University, Changsha 410005 Hunan Province, China*

Bo Sun − *Department of Hepatobiliary Surgery, The First Affiliated Hospital of Hunan Normal University, Changsha 410005 Hunan Province, China*

Yu Jiang − *Central Laboratory, Hunan Provincial People's Hospital (The First Affiliated Hospital of Hunan Normal University), Changsha 410005 Hunan Province, China*

Chaochao Tan − *Department of Clinical Laboratory, Hunan Provincial People's Hospital (The First Affiliated Hospital of Hunan Normal University), Changsha 410005 Hunan Province, China*

Chuang Peng − *Department of Hepatobiliary Surgery, The First Affiliated Hospital of Hunan Normal University, Changsha 410005 Hunan Province, China; Hunan Provincial Key Laboratory of Biliary Disease Prevention and Treatment, Changsha 410005 Hunan Province, China; Clinical Medical Technology Research Center of Hunan Provincial for Biliary Disease Prevention and Treatment, Changsha 410005 Hunan Province, China*

Complete contact information is available at: https://pubs.acs.org/10.1021/acsanm.3c01697

Author Contributions

[▽]Y.L. and R.C. performed the data; X.C., K.C., Y.J., and R.C. contributed significantly to the analysis and manuscript preparation; Y.L., R.C., B.S., and C.T. performed the data analyses and wrote the manuscript; Y.Z. and C.P. contributed to the conception of the study; Y.S., L.W., and S.L. helped perform the analysis with constructive discussions. Y.L. and R.C. contributed equally to this work.

Funding

This work was financially supported by following funds: National Natural Science Foundation of China (no. 81902017), the Huxiang Youth Talent Support Program (no. 2020RC3066), the Natural Science Fund for Excellent Young Scholars of Hunan Province (2021JJ20003), Postgraduate Scientific Research Innovation Project of Hunan Province (CX20220524), and the Project of Improving the Diagnosis and Treatment Capacity of Hepatobiliary, Pancreas and Intestine in Hunan Province (Xiangwei [2019] no. 118).

Notes

The authors declare no competing financial interest.

REFERENCES

(1) Mederos, M. A.; Reber, H. A.; Girgis, M. D. Acute Pancreatitis: A Review. *JAMA* **2021**, *325*, 382−390.

(2) Lee, P. J.; Papachristou, G. I. New insights into acute pancreatitis. *Nat. Rev. Gastroenterol. Hepatol.* **2019**, *16*, 479−496.

(3) Lankisch, P. G.; Apte, M.; Banks, P. A. Acute pancreatitis. *Lancet* **2015**, *386*, 85−96.

(4) Song, Y.; Zhang, Z.; Yu, Z.; Xia, G.; Wang, Y.; Wang, L.; Peng, C.; Jiang, B.; Liu, S. Wip1 Aggravates the Cerulein-Induced Cell Autophagy and Inflammatory Injury by Targeting STING/TBK1/IRF3 in Acute Pancreatitis. *Inflammation* **2021**, *44*, 1175−1183.

(5) Gardner, T. B. Acute Pancreatitis. *Ann. Intern. Med.* **2021**, *174*, ITC17−ITC32.

(6) Garg, P. K.; Singh, V. P. Organ Failure Due to Systemic Injury in Acute Pancreatitis. *Gastroenterology* **2019**, *156*, 2008−2023.

(7) Strum, W. B.; Boland, C. R. Advances in acute and chronic pancreatitis. *World J. Gastroenterol.* **2023**, *29*, 1194−1201.

(8) Schepers, N. J.; Bakker, O. J.; Besselink, M. G.; Ahmed Ali, U.; Bollen, T. L.; Gooszen, H. G.; van Santvoort, H. C.; Bruno, M. J. Impact of characteristics of organ failure and infected necrosis on mortality in necrotising pancreatitis. *Gut* **2019**, *68*, 1044−1051.

(9) Li, Y.; Yin, B.; Song, Y.; Chen, K.; Chen, X.; Zhang, Y.; Yu, N.; Peng, C.; Zhang, X.; Song, G.; Liu, S. A novel ROS-Related chemiluminescent semiconducting polymer nanoplatform for acute pancreatitis early diagnosis and severity assessment. *J. Nanobiotechnol.* **2023**, *21*, 173.

(10) Peng, C.; Tu, G.; Wang, J.; Wang, Y.; Wu, P.; Yu, L.; Li, Z.; Yu, X. MLKL signaling regulates macrophage polarization in acute pancreatitis through CXCL10. *Cell Death Dis.* **2023**, *14*, 155.

(11) Kong, L.; Deng, J.; Zhou, X.; Cai, B.; Zhang, B.; Chen, X.; Chen, Z.; Wang, W. Sitagliptin activates the p62-Keap1-Nrf2 signalling pathway to alleviate oxidative stress and excessive autophagy in severe acute pancreatitis-related acute lung injury. *Cell Death Dis.* **2021**, *12*, 928.

(12) He, J.; Ma, M.; Li, D.; Wang, K.; Wang, Q.; Li, Q.; He, H.; Zhou, Y.; Li, Q.; Hou, X.; Yang, L. Sulfiredoxin-1 attenuates injury and inflammation in acute pancreatitis through the ROS/ER stress/Cathepsin B axis. *Cell Death Dis.* **2021**, *12*, 626.

(13) Ushio-Fukai, M. Compartmentalization of redox signaling through NADPH oxidase-derived ROS. *Antioxid. Redox Signaling* **2009**, *11*, 1289−1299.

(14) Padureanu, V.; Florescu, D. N.; Padureanu, R.; Ghenea, A. E.; Gheonea, D. I.; Oancea, C. N. Role of antioxidants and oxidative stress in the evolution of acute pancreatitis (Review). *Exp. Ther. Med.* **2022**, *23*, 197.

(15) Schoenberg, M. H.; Birk, D.; Beger, H. G. Oxidative stress in acute and chronic pancreatitis. *Am. J. Clin. Nutr.* **1995**, *62*, 1306S−1314S.

(16) Li, H.; Lin, Y.; Zhang, L.; Zhao, J.; Li, P. Ferroptosis and its emerging roles in acute pancreatitis. *Chin. Med. J. (Engl)* **2022**, *135*, 2026−2034.

(17) Fan, R.; Sui, J.; Dong, X.; Jing, B.; Gao, Z. Wedelolactone alleviates acute pancreatitis and associated lung injury via GPX4 mediated suppression of pyroptosis and ferroptosis. *Free Radic. Biol. Med.* **2021**, *173*, 29−40.

(18) Yang, L.; Ye, F.; Liu, J.; Klionsky, D. J.; Tang, D.; Kang, R. Extracellular SQSTM1 exacerbates acute pancreatitis by activating autophagy-dependent ferroptosis. *Autophagy* **2022**, *19*, 1733−1744.

(19) Huang, Y.; Ren, J.; Qu, X. Nanozymes: Classification, Catalytic Mechanisms, Activity Regulation, and Applications. *Chem. Rev.* **2019**, *119*, 4357−4412.

(20) Miao, Z.; Jiang, S.; Ding, M.; Sun, S.; Ma, Y.; Younis, M. R.; He, G.; Wang, J.; Lin, J.; Cao, Z.; Huang, P.; Zha, Z. Ultrasmall Rhodium Nanozyme with RONS Scavenging and Photothermal Activities for Anti-Inflammation and Antitumor Theranostics of Colon Diseases. *Nano Lett.* **2020**, *20*, 3079−3089.

(21) Feng, W.; Han, X.; Hu, H.; Chang, M.; Ding, L.; Xiang, H.; Chen, Y.; Li, Y. 2D vanadium carbide MXenzyme to alleviate ROS-mediated inflammatory and neurodegenerative diseases. *Nat. Commun.* **2021**, *12*, 2203.

(22) Xu, B.; Wang, H.; Wang, W.; Gao, L.; Li, S.; Pan, X.; Wang, H.; Yang, H.; Meng, X.; Wu, Q.; Zheng, L.; Chen, S.; Shi, X.; Fan, K.; Yan, X.; Liu, H. A Single-Atom Nanozyme for Wound Disinfection Applications. *Angew Chem. Int. Ed. Engl.* **2019**, *58*, 4911−4916.

(23) Li, J.; Lu, N.; Han, S.; Li, X.; Wang, M.; Cai, M.; Tang, Z.; Zhang, M. Construction of Bio-Nano Interfaces on Nanozymes for Bioanalysis. *ACS Appl. Mater. Interfaces* **2021**, *13*, 21040−21050.

(24) Shao, F.; Wu, Y.; Tian, Z.; Liu, S. Biomimetic nanoreactor for targeted cancer starvation therapy and cascade amplificated chemotherapy. *Biomaterials* **2021**, *274*, 120869.

(25) Wu, J.; Wang, X.; Wang, Q.; Lou, Z.; Li, S.; Zhu, Y.; Qin, L.; Wei, H. Nanomaterials with enzyme-like characteristics (nanozymes):

next-generation artificial enzymes (II). *Chem. Soc. Rev.* **2019**, *48*, 1004−1076.
(26) Wu, Y.; Chen, Z.; Yao, Z.; Zhao, K.; Shao, F.; Su, J.; Liu, S. Black Phosphorus Quantum Dots Encapsulated Biodegradable Hollow Mesoporous MnO2: Dual-Modality Cancer Imaging and Synergistic Chemo-Phototherapy. *Adv. Funct. Mater.* **2021**, *31*, 2104643.
(27) Zhang, D. Y.; Liu, H.; Zhu, K. S.; He, T.; Younis, M. R.; Yang, C.; Lei, S.; Wu, J.; Lin, J.; Qu, J.; Huang, P. Prussian blue-based theranostics for ameliorating acute kidney injury. *J. Nanobiotechnol.* **2021**, *19*, 266.
(28) Li, D.; Liu, M.; Li, W.; Fu, Q.; Wang, L.; Lai, E.; Zhao, W.; Zhang, K. Synthesis of Prussian Blue Nanoparticles and Their Antibacterial, Antiinflammation and Antitumor Applications. *Pharmaceuticals (Basel)* **2022**, *15*, 769.
(29) Khurana, A.; Anchi, P.; Allawadhi, P.; Kumar, V.; Sayed, N.; Packirisamy, G.; Godugu, C. Superoxide dismutase mimetic nanoceria restrains cerulein induced acute pancreatitis. *Nanomedicine (Lond)* **2019**, *14*, 1805−1825.
(30) Ye, C.; Zhang, W.; Zhao, Y.; Zhang, K.; Hou, W.; Chen, M.; Lu, J.; Wu, J.; He, R.; Gao, W.; Zheng, Y.; Cai, X. Prussian Blue Nanozyme Normalizes Microenvironment to Delay Osteoporosis. *Adv. Healthcare Mater.Adv. Healthcare Mater.* **2022**, *11*, No. e2200787.
(31) Zhang, B.; Chen, G.; Wu, X.; Li, Y.; Xiao, Y.; Li, J.; He, L.; Li, Y.; Wang, S.; Zhao, J.; Liu, C.; Zhou, H.; Li, Y.; Pei, X. Biomimetic Prussian blue nanozymes with enhanced bone marrow-targeting for treatment of radiation-induced hematopoietic injury. *Biomaterials* **2023**, *293*, 121980.
(32) Zhang, K.; Wu, J.; Zhao, X.; Qin, J.; Xue, Y.; Zheng, W.; Wang, L.; Wang, H.; Shen, H.; Niu, T.; Luo, Y.; Tang, R.; Wang, B. Prussian Blue/Calcium Peroxide Nanocomposites-Mediated Tumor Cell Iron Mineralization for Treatment of Experimental Lung Adenocarcinoma. *ACS Nano* **2021**, *15*, 19838−19852.
(33) Lennicke, C.; Cocheme, H. M. Redox metabolism: ROS as specific molecular regulators of cell signaling and function. *Mol. Cell* **2021**, *81*, 3691−3707.
(34) Han, L.; Li, C.; Zhang, T.; Lang, Q.; Liu, A. Au@Ag Heterogeneous Nanorods as Nanozyme Interfaces with Peroxidase-Like Activity and Their Application for One-Pot Analysis of Glucose at Nearly Neutral pH. *ACS Appl. Mater. Interfaces* **2015**, *7*, 14463−14470.
(35) Liu, Y.; Wang, X.; Li, X.; Qiao, S.; Huang, G.; Hermann, D. M.; Doeppner, T. R.; Zeng, M.; Liu, W.; Xu, G.; Ren, L.; Zhang, Y.; Liu, W.; Casals, E.; Li, W.; Wang, Y. C. A Co-Doped Fe(3)O(4) Nanozyme Shows Enhanced Reactive Oxygen and Nitrogen Species Scavenging Activity and Ameliorates the Deleterious Effects of Ischemic Stroke. *ACS Appl. Mater. Interfaces* **2021**, *13*, 46213−46224.
(36) He, M. T.; Park, H. S.; Kim, Y. S.; Lee, A. Y.; Cho, E. J. Protective Effect of Membrane-Free Stem Cells against Lipopolysaccharide and Interferon-Gamma-Stimulated Inflammatory Responses in RAW 264.7 Macrophages. *Int. J. Mol. Sci.* **2021**, *22*, 6894.
(37) Zhu, H.; Tamura, T.; Fujisawa, A.; Nishikawa, Y.; Cheng, R.; Takato, M.; Hamachi, I. Imaging and Profiling of Proteins under Oxidative Conditions in Cells and Tissues by Hydrogen-Peroxide-Responsive Labeling. *J. Am. Chem. Soc.* **2020**, *142*, 15711−15721.
(38) Sah, R. P.; Garg, P.; Saluja, A. K. Pathogenic mechanisms of acute pancreatitis. *Curr. Opin. Gastroenterol.* **2012**, *28*, 507−515.
(39) Xue, Q.; Yan, D.; Chen, X.; Li, X.; Kang, R.; Klionsky, D. J.; Kroemer, G.; Chen, X.; Tang, D.; Liu, J. Copper-dependent autophagic degradation of GPX4 drives ferroptosis. *Autophagy* **2023**, *19*, 1982−1996.

https://doi.org/10.1021/acsanm.3c01697
ACS Appl. Nano Mater. 2023, 6, 12968−12979